ADVANCED MATERIALS
www.advmat.de

Massively Evoking Immunogenic Cell Death by Focused Mitochondrial Oxidative Stress using an AIE Luminogen with a Twisted Molecular Structure

*Chao Chen, Xiang Ni, Shaorui Jia, Yong Liang, Xiaoli Wu, Deling Kong, and Dan Ding**

Immunogenic cell death (ICD) provides momentous theoretical principle for modern cancer immunotherapy. However, the currently available ICD inducers are still very limited and photosensitizer-based ones can hardly induce sufficient ICD to achieve satisfactory cancer immunotherapy by themselves. Herein, an organic photosensitizer (named TPE-DPA-TCyP) with a twisted molecular structure, strong aggregation-induced emission activity, and specific ability is reported for effectively inducing focused mitochondrial oxidative stress of cancer cells, which can serve as a much superior ICD inducer to the popularly used ones, including chlorin e6 (Ce6), pheophorbide A, and oxaliplatin. Furthermore, more effective in vivo ICD immunogenicity of TPE-DPA-TCyP than Ce6 is also demonstrated using a prophylactic tumor vaccination model. The underlying mechanism of the effectiveness and robustness of TPE-DPA-TCyP in inducing antitumor immunity and immune-memory effect in vivo is verified by immune cell analyses. This study thus reveals that inducing focused mitochondrial oxidative stress is a highly effective strategy to evoke abundant and large-scale ICD.

C. Chen, Dr. X. Ni, S. Jia, Prof. D. Kong, Prof. D. Ding
State Key Laboratory of Medicinal Chemical Biology
Key Laboratory of Bioactive Materials
Ministry of Education, and College of Life Sciences
Nankai University
Tianjin 300071, China
E-mail: dingd@nankai.edu.cn

Dr. Y. Liang
Department of Clinical Laboratory
Huai'an Hospital Affiliated to Xuzhou Medical University and Huai'an Second Hospital
Huai'an 223002, Jiangsu, China

Dr. X. Wu
School of Life Sciences
Tianjin University
Tianjin 300072, China

Prof. D. Kong, Prof. D. Ding
Jiangsu Center for the Collaboration and Innovation of Cancer Biotherapy
Cancer Institute
Xuzhou Medical University
Xuzhou 221002, Jiangsu, China

The ORCID identification number(s) for the author(s) of this article can be found under https://doi.org/10.1002/adma.201904914.

DOI: 10.1002/adma.201904914

The notion of immunogenic cell death (ICD) that is a type of apoptotic cell demise featuring the emission of immunostimulatory damage-associated molecular patterns (DAMPs; e.g., surface-exposed calreticulin) provides momentous theoretical principle for modern cancer immunotherapy.[1] ICD process is capable of reversing the poor immunogenicity suffered by many cancers such as metastatic triple negative breast cancer, making them susceptible for immunotherapy.[2] Although the ICD mechanism is comprehensive, one of the most important hallmark events is the translocation of calreticulin (CRT) from endoplasmic reticulum (ER) to the surface of dying cells, which becomes a vital signal for professional antigen-presenting cells (APCs) such as dendritic cells (DCs) to phagocytose the corpses and debris of cancer cells, and then acts as a natural adjuvant to promote DC maturation and assist the presentation of tumor-associated antigens to T cells in lymph nodes, hence initiating the adaptive antitumor immunity.[3] Due to the pivotal role of ICD in cancer immunotherapy, the development of the agents that can induce ICD of cancer cells has been attracting considerable interest during the past decade since the concept of ICD emerged.[2,4] Unfortunately, the currently available ICD inducers are still very limited.[5] For example, among such a huge amount of chemotherapeutic drugs, only several ones including methotrexate, doxorubicin, and oxaliplatin can induce obvious surface-exposed CRT (namely ecto-CRT).[6,7] Besides, other reported ICD inducers mainly include oncolytic virus, epidermal growth factor receptor-specific antibodies, γ-/ultraviolet C irradiation, and a few photosensitizers.[8]

Among the versatile ICD inducers, photosensitizers that can produce reactive oxygen species (ROS) after absorbing light hold the merits in terms of in situ photodynamic therapy (PDT) capacity, excellent spatiotemporal precision, negligible toxicity to normal tissues, etc.[9] To date, only a small amount of photosensitizers such as pheophorbide A (PPa), temoporfin, chlorin e6 (Ce6), and hypericin have been reported to be able to evoke ICD of cancer cells to some extent through causing oxidative stress upon light irradiation.[10,11] However, according to the literature, currently available photosensitizers could hardly induce sufficient ecto-CRT to achieve satisfactory cancer

immunotherapy by themselves. For instance, although Ce6 is known as an outstanding photosensitizer-based ICD inducer to generate ecto-CRT, it has been reported that adding exogenous recombinant CRT in Ce6-PDT-based vaccine could significantly enhance the immunotherapy efficacy against cancer,[12] demonstrating that there is still large room for the photosensitizer to evoke antitumor immunity more effectively if realizing more ecto-CRT induction. Furthermore, the widely investigated combined strategies using both the aforementioned photosensitizers and immune checkpoint inhibitors (e.g., anti-CTAL4 and anti-PD-L1) also imply that these photosensitizers alone fail to induce strong enough immunogenicity of ICD.[13] Thereby, development of alternative photosensitizers with significantly improved induction of ICD and ecto-CRT is highly desirable.

Despite of the complex causes, one of the main reasons for the unsatisfied ICD induction is that most of the currently reported ICD-inducing photosensitizers are in planar molecular structure, thus leading to highly reduced ROS generation efficiency in aqueous/cellular environment due to the significant intermolecular interactions (e.g., π–π stacking) opening the nonradiative pathway of the excited state.[14] The emergence of photosensitizers with aggregation-induced emission (AIE) characteristics has provided a solution. The AIE luminogens/photosensitizers are usually featured with peripheral intramolecular motion units (e.g., phenyl rings as rotors) and 3D molecular structure.[15] In biological conditions, they are prone to aggregation and their 3D molecular structure enables significantly decreased intermolecular interactions. Meanwhile, aggregation also restricts the excited-state intramolecular motion due to the steric hindrance. These make as much absorbed excitation energy as possible used for fluorescence emission and/or ROS production.[16] As a result, the AIE photosensitizers always show rather effective intracellular ROS generation ability. Although there have been extensive studies on AIE so far, none of them linked AIE photosensitizers and ICD together.

More importantly, we speculated that intracellular oxidative stress in a specific organelle might play a decisive role in evoking ICD. Nevertheless, except that focused ER oxidative stress has been proved to be efficacious to induce ICD,[2,17] there are no previous reports revealing the relationship between oxidative stress in other organelles and ICD. It has been well established that mitochondrion is an extremely important organelle closely engaged in cellular stress signaling,[18] we are hence motivated to study the role of mitochondrial oxidative stress in ICD induction, which has never been investigated so far, to our knowledge.

In this contribution, we report for the first time that inducing focused mitochondrial oxidative stress is a unique way to evoke abundant and large-scale ICD. We start with the design and synthesis of two new mitochondrial targeting AIE photosensitizers (named TPE-DPA-TCyP and DPA-TCyP, respectively, **Figure 1**A) with D-π-A structure and rich intramolecular motion units. Both TPE-DPA-TCyP and DPA-TCyP are weakly emissive in aqueous solutions but emit intense far-red/near-infrared (FR/NIR) fluorescence selectively in cancer cell mitochondria. As compared to DPA-TCyP, TPE-DPA-TCyP is designed to possess more twisted molecular structure and larger HOMO (highest occupied molecular orbital)–LUMO (lowest unoccupied molecular orbital) separation, resulting in stronger AIE activity, weaker intermolecular interactions in aggregates, and higher ROS generation capability, which thus serve as a far better ICD inducer. Furthermore, TPE-DPA-TCyP that causes focused mitochondrial oxidative stress under light excitation is able to greatly amplify ICD induction when compared with its nanoparticle (NP) formulation (Pluronic F127 as the encapsulation matrix), which cannot distribute in mitochondria as well as the widely reported high-performing ICD inducers such as Ce6, PPa, and oxaliplatin. Subsequently, prophylactic tumor vaccination experiment reveals the much more effective in vivo ICD immunogenicity of TPE-DPA-TCyP than Ce6. Finally, the underlying mechanism of TPE-DPA-TCyP-treated tumor cell vaccine for long-lasting effect of antitumor immunity in vivo was demonstrated by immune cell analyses. This work thus provides new insights and materials in the fields of ICD and cancer immunotherapy as well as a useful molecular design guideline for highly effective photosensitizer-based ICD inducers.

The compounds DPA-TCyP and TPE-DPA-TCyP were rationally designed and synthesized according to the synthetic route as illustrated in Figure 1A. Buchwald–Hartwig amination of commercially available 2-bromothiophene with diarylamine 1 gave compound 2, which was formylated via the Vilsmeier–Haack reaction to give corresponding carbaldehyde 3. Compound 5 was afforded by Knoevenagel condensation of compound 3 with compound 4 under basic condition, followed by methylation with CH_3I to yield DPA-TCyP and TPE-DPA-TCyP, respectively. All intermediates and target compounds were characterized by ^{1}H NMR, ^{13}C NMR, and HRMS to confirm their identity and purity (Figures S1–S18, Supporting Information).

In our design strategy, cyanostyrylthiophene core is adopted as both the AIE skeleton and π-linker. By combination of the diarylaminothienyl block as strong electronic donor (D) and pyridinium unit as both the electronic acceptor (A) and efficient mitochondrial targeting moiety, a D–π–A structure is built. The absorption and emission spectra of TPE-DPA-TCyP and DPA-TCyP in dimethyl sulfoxide (DMSO, good solvent) are displayed in Figure S19 (Supporting Information). TPE-DPA-TCyP and DPA-TCyP show a large absorption peak at 504 and 496 nm and an FR/NIR emission centered at 697 and 690 nm, respectively. After gradual addition of the poor solvent toluene to the DMSO solution that enables aggregate formation, both the fluorescence intensities of TPE-DPA-TCyP and DPA-TCyP have a main trend to increase with increasing the toluene fraction in DMSO/toluene mixture, demonstrating that both TPE-DPA-TCyP and DPA-TCyP are AIE luminogens (AIEgens). Noteworthy, thanks to the integration of tetraphenylethene (TPE) unit, the AIE activity of TPE-DPA-TCyP is much stronger than that of DPA-TCyP, when comparing their ratio of maximum fluorescence intensity in DMSO/toluene mixture with 90% toluene fraction to that in pure DMSO (Figure S19, Supporting Information).

Figure 1B shows the emission spectra of TPE-DPA-TCyP and DPA-TCyP in aqueous solution. Both the AIEgens are weakly emissive in phosphate buffered saline (PBS). After adding the lipid vesicles that can mimic the mitochondrial membrane environment[19] to the PBS solution, the AIEgen fluorescence greatly turns on and the intensities are about ninefold enhancement for both TPE-DPA-TCyP and DPA-TCyP (Figure 1B). Due to the positive charge of pyridinium, the AIEgens have relatively

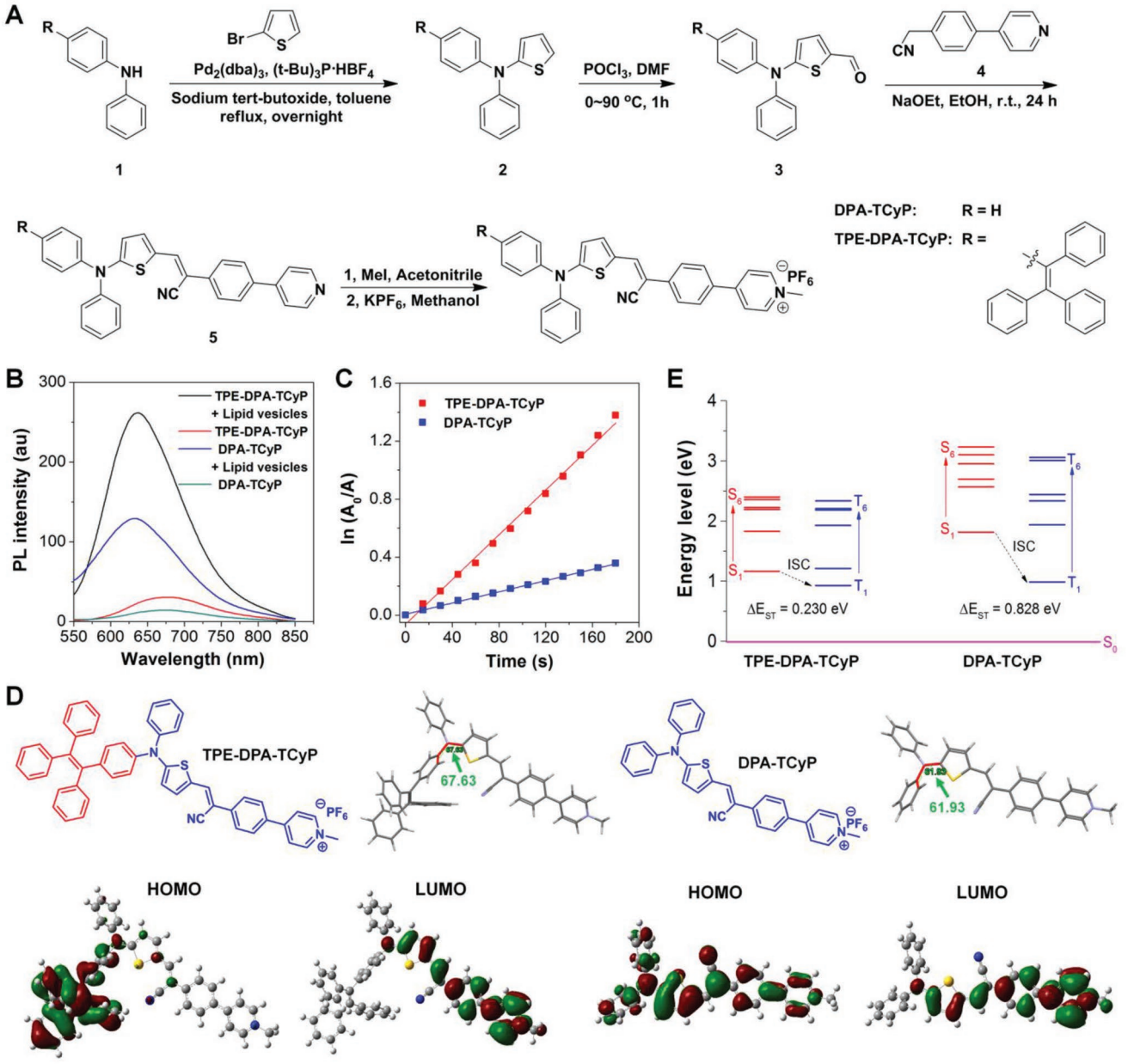

Figure 1. A) Synthetic route to TPE-DPA-TCyP and DPA-TCyP. B) Photoluminescence (PL) spectra of TPE-DPA-TCyP and DPA-TCyP (10×10^{-6} M) in the presence and absence of lipid vesicles (22×10^{-6} M) in PBS. C) Plot of $\ln(A_0/A)$ against light exposure time, where A_0 and A are the ABDA absorbance (378 nm) before and after irradiation, respectively. D) Chemical structures, dihedral angles, and HOMO–LUMO distributions by DFT calculations of TPE-DPA-TCyP and DPA-TCyP. E) Energy levels of S_1–S_6 and T_1–T_6 calculated by the vertical excitation of the optimized structures in (D).

good water-solubility. Thus, the free excited-state intramolecular motions including the rotation of phenyl rings and the twisting between D and A (twisted intramolecular charge transfer (TICT) process) consume the absorbed excitation energy via nonradiative decay, making TPE-DPA-TCyP and DPA-TCyP weakly fluoresce in aqueous media. Since it is well-known that cancer cells possess rather high negative mitochondrial membrane potential,[19] the electrostatic interaction enables the aggregation of AIEgens in the mitochondrial membrane. This effectively restricts the above-mentioned intramolecular motions in the excited states, as evidenced by the ≈45 nm blueshift of the AIEgen emission after addition of lipid vesicles owing to the restricted intramolecular twisting suppressing TICT, which results in significant fluorescence switch-on.

As the effective ROS generation capacity is an essential prerequisite for photosensitizer-based ICD inducer, we next investigated and compared the ROS production of TPE-DPA-TCyP and DPA-TCyP in aqueous solution under white light irradiation (10 mW cm^{-2}) with 9,10-anthracenediyl-bis(methylene) dimalonic acid (ABDA) as the ROS indicator. From the slopes of the plots depicted in Figure 1C, ABDA decomposition rate constants for TPE-DPA-TCyP and DPA-TCyP are calculated to

be 0.00771 and 0.00193 s^{-1}, respectively, indicating that TPE-DPA-TCyP is a much more efficient photosensitizer. It is also verified that TPE-DPA-TCyP exhibits higher ROS generation efficiency than Ce6 (Figure S20, Supporting Information). To deeply understand the mechanism of superior ROS production ability of TPE-DPA-TCyP to DPA-TCyP, density functional theory (DFT) calculations were performed. As shown in Figure 1D,E, plenty of overlap between HOMO and LUMO is observed for DPA-TCyP with a relatively large ΔE_{ST} (the energy gap between the lowest singlet (S_1) and triplet excited state (T_1)) of 0.828 eV. Interestingly, by incorporation of TPE unit into the diarylamine structure, the HOMO of TPE-DPA-TCyP is almost totally localized over the TPEamino group and its LUMO is primarily distributed over cyanostyrylthiophene core and pyridinium unit. It has been reported that effective separation of HOMO–LUMO distribution can reduce ΔE_{ST},[20] which agrees well with the calculation result for TPE-DPA-TCyP with a far lower ΔE_{ST} value of 0.230 eV (Figure 1E). Because of the highly reduced ΔE_{ST}, the intersystem crossing (ISC) efficiency is remarkably improved, which underlies the superior ROS generation capability of TPE-DPA-TCyP.

The photoluminescence (PL) quantum yields (QYs) of TPE-DPA-TCyP and DPA-TCyP in the solid state were determined to be 6.3% and 3.6%, respectively, using a calibrated integrating sphere. It has been well accepted that the absorbed excitation energy is mainly dissipated through 3 routes, i.e., fluorescence via radiation pathway, ISC to T_1 followed by production of ROS and/or phosphorescence, as well as thermal deactivation through nonradiative decay.[21] As illustrated in Figure 1D and Figure S21 (Supporting Information), the optimized geometric structures calculated by DFT reveal that compared with DPA-TCyP, TPE-DPA-TCyP has a much more 3D twisted molecular structure. The dihedral angle between thiophene and benzene rings is 61.93° in DPA-TCyP. With a crowded TPE group attaching to the benzene ring, the whole structure becomes more twisted. For example, the same dihedral angle increases to 67.63° in TPE-DPA-TCyP. The more twisted molecular structure undoubtedly decreases the intermolecular interactions such as π–π stacking (nonradiative decay) in the aggregated/solid state more effectively, making the absorbed energy saved for the other two pathways. This hence reasonably explains why TPE-DPA-TCyP shows higher fluorescence QY and ROS generation capability than DPA-TCyP (neither TPE-DPA-TCyP nor DPA-TCyP emits phosphorescence), which also highlights the importance of our molecular design approach to advanced photosensitizer in terms of D-π-A structure, introduction of intramolecular motion units, enhancement of the 3D twisted molecular structure and separation of HOMO–LUMO distribution. As a consequence, TPE-DPA-TCyP was then selected for the next ICD induction experiments.

In this work, we aimed to study the relationship between ICD and focused mitochondrial oxidative stress. The specific mitochondrial targeting ability of TPE-DPA-TCyP is thereby important, which was then assessed with metastatic triple negative breast cancer cells (murine 4T1). It is noted that TPE-DPA-TCyP has negligible cytotoxicity against 4T1 cancer cells in dark (Figure S22, Supporting Information). As shown in the confocal laser scanning microscopy (CLSM) images (**Figure 2**A), after incubation of 4T1 cancer cells with TPE-DPA-TCyP at 37 °C for 90 min, TPE-DPA-TCyP is chiefly distributed in mitochondria and lights up its fluorescence, which is confirmed by the excellent fluorescence overlap with commercial MitoTracker Deep Red FM (large overlap coefficient of 0.839 determined by Image Pro Plus software, Figure 2B). After verification of mitochondrial anchoring, we investigated whether TPE-DPA-TCyP could generate ROS within cancer cells using 2′,7′-dichlorodihydrofluorescein diacetate (DCF-DA) as the indicator. It is obvious that bright intracellular green fluorescence from the reaction between DCF-DA and ROS is seen after white light irradiation (10 mW cm^{-2}, 1 min) with the TPE-DPA-TCyP-treated 4T1 cells (Figure S23, Supporting Information). Such green fluorescence can be largely vanished when *N*-acetylcysteine (NAC), an antioxidant, is employed to scavenge the light-triggered ROS. The result demonstrates the effective ROS production of TPE-DPA-TCyP in cancer cellular mitochondria.

We next studied whether our mitochondrion-targeting photosensitizer could massively evoke ICD through immunostaining analysis of ecto-CRT on the cancer cell surface, which is known as a golden standard to estimate ICD induction.[11] Upon successive treatment with TPE-DPA-TCyP (0.2×10^{-6} M) at 37 °C for 90 min and while light irradiation (10 mW cm^{-2}) for 1 min, rather high ecto-CRT expression can be visualized by its immunofluorescence. When fixing the compound incubation time, light irradiation time and light power density, as low as 50×10^{-9} M of TPE-DPA-TCyP remains to be able to induce ecto-CRT efficiently (Figure S24, Supporting Information), indicating the superb capacity of TPE-DPA-TCyP to evoke ICD.

To investigate whether such vast amount of ecto-CRT expression mainly rooted in the focused mitochondrial oxidative stress, we altered the cancer intracellular distribution of TPE-DPA-TCyP against mitochondria via doping the AIEgen into NPs. To this end, an amphiphilic co-polymer, Pluronic F127, was used as the encapsulation matrix to formulate TPE-DPA-TCyP into NPs by a nanoprecipitation approach.[22] The resultant TPE-DPA-TCyP NPs have a nearly spherical shape with a mean hydrodynamic diameter of ≈126 nm (Figure S25, Supporting Information). The PL QY of TPE-DPA-TCyP NPs in water is determined to be ≈2.8% using 4-(dicyanomethylene)-2-methyl-6-(p-dimethylaminostyryl)-4H-pyran in methanol (QY = 0.43) as the standard, which is significantly higher than that of pure TPE-DPA-TCyP (≈1.0%) due to NP formulation restricting the intramolecular motion. After incubation with TPE-DPA-TCyP NPs (0.72×10^{-6} M based on TPE-DPA-TCyP) at 37 °C for 90 min, 4T1 cancer cells were imaged by CLSM. The result in Figure 2A reveals that an overwhelming number of the TPE-DPA-TCyP NPs are not located in the mitochondria because of the NP formulation, as indicated by the poor overlap between the TPE-DPA-TCyP fluorescence and that of MitoTracker Deep Red FM with a quite small overlap coefficient of 0.099 (Figure 2B).

It is worthy to note that neither NP formulation nor lipid vesicle addition has negligible interference on the ROS generation ability of TPE-DPA-TCyP, as evidenced by nearly the same ABDA decline rates upon light irradiation to TPE-DPA-TCyP itself, NPs, and "TPE-DPA-TCyP + lipid vesicles," respectively (Figure S26, Supporting Information). Furthermore, for reasonable comparison, the same compound internalization by cells for TPE-DPA-TCyP and TPE-DPA-TCyP NPs must be realized. Therefore, we fixed the incubation concentration of pure

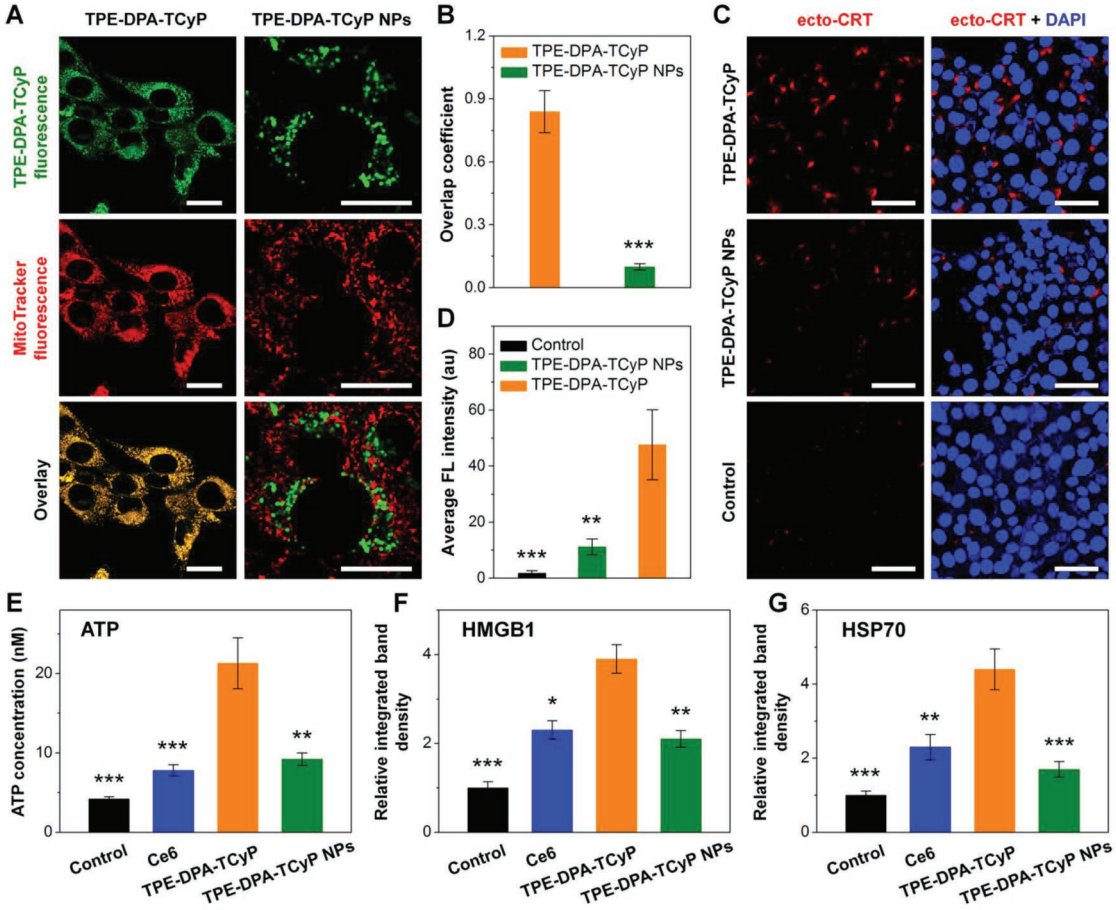

Figure 2. A) CLSM images of 4T1 cancer cells treated with TPE-DPA-TCyP or TPE-DPA-TCyP NPs, which were co-stained with commercial MitoTracker Deep Red FM. Scale bars, 20 μm. B) The overlap coefficient between the TPE-DPA-TCyP/TPE-DPA-TCyP NPs fluorescence and MitoTracker Deep Red FM fluorescence, based on the typical images in (A). C) CLSM images display the ecto-CRT expression (red fluorescence) of 4T1 cells after incubation with TPE-DPA-TCyP (0.2×10^{-6} M) and TPE-DPA-TCyP NPs (0.72×10^{-6} M), respectively, at 37 °C for 90 min and subsequent light irradiation (10 mW cm^{-2}) for 1 min. The cell nuclei were stained by 4′,6-diamidino-2-phenylindole (DAPI; blue fluorescence). Scale bars, 50 μm. D) The average fluorescence (FL) intensity of ecto-CRT immunofluorescence, based on the typical images in (C). E–G) Quantitative analyses of ATP (E), HMGB1 (F), and HSP70 (G) in the cell supernatants after 4T1 cells were treated with various photosensitizers indicated and subsequent light exposure, respectively. *** $P < 0.001$, ** $P < 0.01$, and * $P < 0.05$, in comparison with "TPE-DPA-TCyP" group in (B), (D), and (E–G).

TPE-DPA-TCyP as 0.2×10^{-6} M and optimized that of TPE-DPA-TCyP NPs to make sure the coincident cell uptake of TPE-DPA-TCyP. After each agent treatment, the 4T1 cells were washed and lysed, and then the TPE-DPA-TCyP amount in cell lysates was determined by its absorption spectrum. It is found that when 0.72×10^{-6} M (based on TPE-DPA-TCyP) of TPE-DPA-TCyP NPs are incubated with 4T1 cells at 37 °C for 90 min, the intracellular TPE-DPA-TCyP amount is nearly the same with that in pure TPE-DPA-TCyP (0.2×10^{-6} M, 90 min)-incubated cells (Figure S27, Supporting Information), which is also confirmed by the virtually identical intracellular ROS level when two cells are exposed to light irradiation using DCF-DA as the ROS indicator (Figure S28, Supporting Information).

Upon white light irradiation (10 mW cm^{-2}, 1 min) of the pure TPE-DPA-TCyP (0.2×10^{-6} M)-treated and TPE-DPA-TCyP NP (0.72×10^{-6} M)-treated 4T1 cells, the expressions of ecto-CRT were detected and compared using CLSM. As shown in Figure 2C, although TPE-DPA-TCyP NPs are capable of obviously inducing ecto-CRT, the ecto-CRT amount is far less than that induced by pure TPE-DPA-TCyP. Quantitatively, the average fluorescence intensity from TPE-DPA-TCyP NP-induced ecto-CRT proteins is ≈4.3-fold lower than that of pure TPE-DPA-TCyP-induced ones (Figure 2D). Besides ecto-CRT, other DAMPs of ICD including secreted ATP, released high mobility group protein B1 (HMGB1) and heat shock protein 70 (HSP70) were also investigated. As shown in Figure 2E–G and Figure S29 (Supporting Information), significantly higher levels of ATP, HMGB1, and HSP70 are found in the 4T1 cellular supernatants after treatment with "TPE-DPA-TCyP (0.2×10^{-6} M) + light irradiation" than "TPE-DPA-TCyP NPs (0.72×10^{-6} M) + light irradiation." Thus, it is reasonable to conclude that such tremendous disparity in emission of various DAMPs is attributed to the specific mitochondrial distribution, and that ROS-induced mitochondrial stress is a new and extremely effective strategy to magnify ICD.

The ICD evoking ability of TPE-DPA-TCyP was then compared with the currently available photosensitizers including Ce6 and PPa that are reported as high-performing

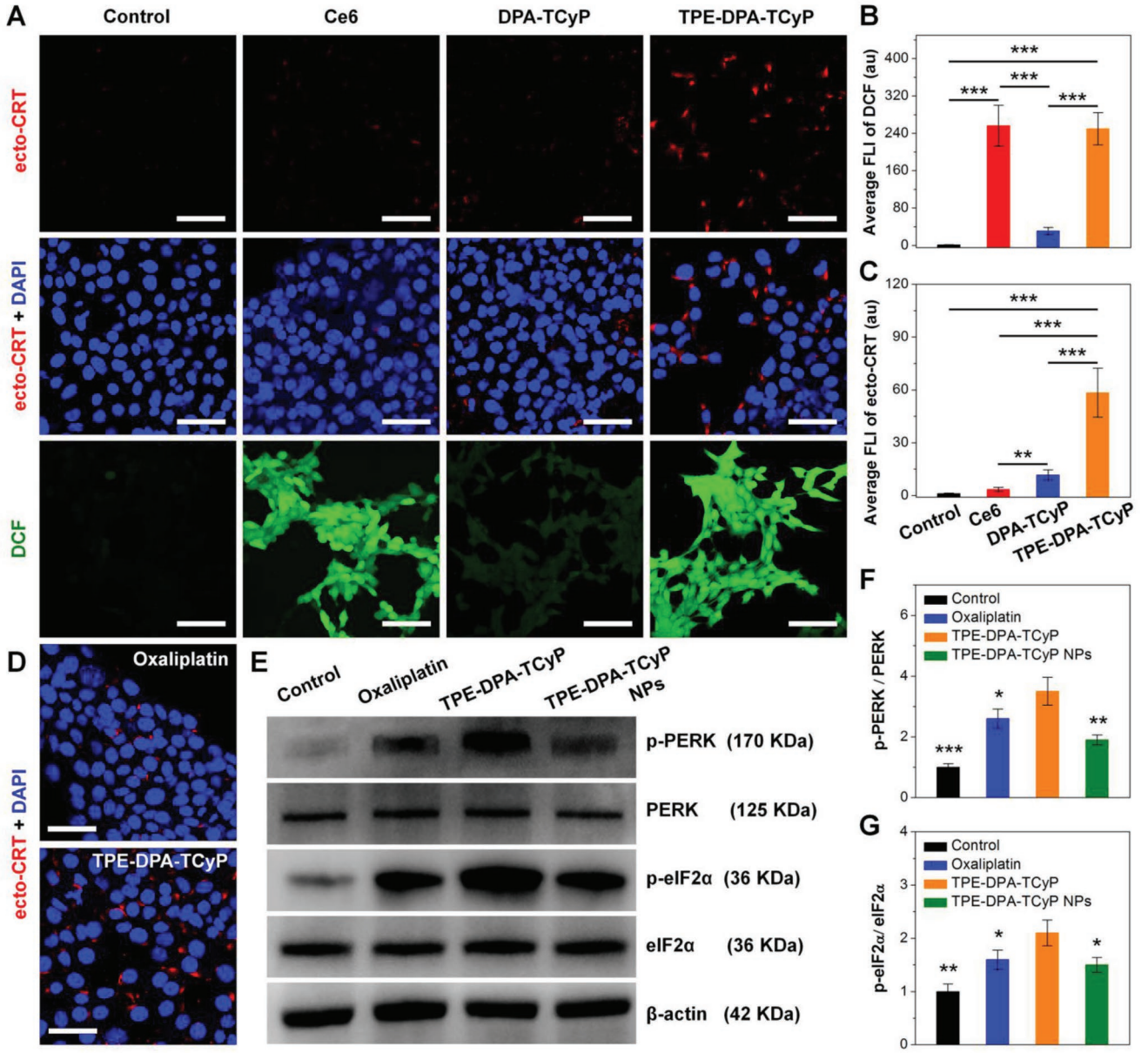

Figure 3. A) CLSM images show the ecto-CRT expression (red fluorescence) and the intracellular ROS levels (green fluorescence from dichlorofluorescein (DCF) by the reaction between DCF-DA and ROS) of 4T1 cancer cells received various treatments. Scale bars, 50 μm. B,C) Quantitative data indicate the average fluorescence intensity (FLI) of DCF (B) and ecto-CRT (C), based on the typical images in (A). *** $P < 0.001$ and ** $P < 0.01$. D) CLSM images show the ecto-CRT levels (red fluorescence) of 4T1 cancer cells treated with oxaliplatin (5×10^{-6} M) and "TPE-DPA-TCyP + light irradiation," respectively. Scale bars, 50 μm. E) Representative immunoblots indicate different protein levels from each treatment group indicated. F,G) Quantitative analyses of the ratios of p-PERK/PERK (F) and p-eIF2α/eIF2α (G), based on the typical images in (E). *** $P < 0.001$, ** $P < 0.01$, and * $P < 0.05$, in comparison with "TPE-DPA-TCyP" group in (F,G).

ICD inducers.[10,11] The qualitative and quantitative results in **Figure 3**A,B suggest that the treatment of "0.5×10^{-6} M of Ce6 + light irradiation (10 mW cm^{-2}, 1 min)" can lead to nearly the same ROS level within 4T1 cells as "0.2×10^{-6} M of TPE-DPA-TCyP + light irradiation (10 mW cm^{-2}, 1 min)." Moreover, 0.2×10^{-6} M of TPE-DPA-TCyP and 0.5×10^{-6} M of Ce6 show similar PDT efficacy against 4T1 cancer cells by 3-(4,5-dimethylthiazol-2-yl)-2,5-diphenyl tetrazolium bromide (MTT) assay (Figure S30, Supporting Information), which are hence comparable in evaluation of ICD. As displayed in Figures 2E,G and 3A,C, compared with Ce6, PDT with TPE-DPA-TCyP results in far more emission of DAMPs (e.g., ≈17.4-fold higher ecto-CRT level on the 4T1 cell surface), despite of the same intracellular ROS generation. Furthermore, TPE-DPA-TCyP also exhibits far higher ecto-CRT expression than PPa after light exposure (Figure S31, Supporting Information). This results not only prove that TPE-DPA-TCyP is a superior photosensitizer-based ICD inducer to the popularly used ones, but also further corroborate the importance of mitochondrial oxidative stress in boosting ICD.

DPA-TCyP that is able to anchor mitochondria as well (Figure S32, Supporting Information), is also used as a control. The 4T1 cells were incubated with TPE-DPA-TCyP and DPA-TCyP (0.2×10^{-6} M for each compound), respectively, at 37 °C for 90 min, which was followed by light irradiation (10 mW cm^{-2}, 1 min). As revealed in Figure 3A,C, both the intracellular ROS generation and ecto-CRT expression by DPA-TCyP are significantly lower than those by TPE-DPA-TCyP, demonstrating that more effective ROS production ability in mitochondria is beneficial to ICD induction. This thus once again emphasizes the advantage of our molecular design for TPE-DPA-TCyP. Noteworthy, under the same experimental condition, the cell surface ecto-CRT level of DPA-TCyP (0.2×10^{-6} M)-treated 4T1 cells is even significantly higher than that of Ce6 (0.5×10^{-6} M)-treated cells (Figure 3A,C), although the intracellular ROS production by DPA-TCyP upon light irradiation is far less than that by Ce6 (Figure 3A,B). This result further confirms the essentiality of ROS-induced mitochondrial stress in massively evoking ICD. Finally, oxaliplatin, an extensively reported effective ICD inducer,[7] was also employed as a positive control. In this experiment, 5×10^{-6} M of oxaliplatin was used to treat 4T1 cancer cells, as this concentration was demonstrated to be ideal for inducing ICD.[7] However, the ecto-CRT level induced by oxaliplatin is much lower than that by TPE-DPA-TCyP (0.2×10^{-6} M) with light exposure (10 mW cm^{-2}, 1 min), as depicted in Figure 3D. These data together manifest that TPE-DPA-TCyP is an advanced ICD inducer thanks to the specific targeting and efficient ROS production in the cancer cell mitochondria.

According to the literature, PERK-mediated eIF2α phosphorylation is a well-accepted signal pathway to understand the mechanism behind the ICD inducers including UVC irradiation, methotrexate, and oxaliplatin.[23] Therefore, we analyzed the relevant protein levels upon treatment with "TPE-DPA-TCyP (0.2×10^{-6} M) + light irradiation" and "TPE-DPA-TCyP NPs (0.72×10^{-6} M) + light irradiation," respectively, by western blot. Oxaliplatin as an ICD inducer with relatively clear signal pathway was used as a control. As shown in Figure 3E,G, similar to oxaliplatin, both the PDTs of TPE-DPA-TCyP and TPE-DPA-TCyP NPs can up-regulate the phosphorylation levels of PERK and eIF2α as well. Moreover, much higher protein levels of p-PERK and p-eIF2α are observed in "TPE-DPA-TCyP + light irradiation" group when comparison with those in "TPE-DPA-TCyP NPs + light irradiation" group and "oxaliplatin" group. These comparison data demonstrate that focused mitochondrial oxidative stress is able to up-regulate the pathway of PERK-mediated eIF2α phosphorylation, which hence amplifies the ICD induction.

The in vivo distribution and toxicity of TPE-DPA-TCyP were investigated using healthy BALB/c mice. It is found that TPE-DPA-TCyP is mainly distributed in lung, liver, stomach and intestine at 1 h post intravenous injection and most of the molecules could be excreted from the mouse body after 48 h (Figure S33, Supporting Information). Additionally, the data in terms of blood chemistry tests and histological analyses of important normal organs indicate that TPE-DPA-TCyP after intravenous administration has rather low in vivo toxicity even at the concentration as high as 300×10^{-6} M (Figures S34–S36, Supporting Information). After verification of the good biosafety, the in vivo ICD immunogenicity of our new developed ICD inducer was next studied using a prophylactic tumor vaccination model, which is a golden standard to assess ICD in vivo.[1,2] Murine 4T1 cancer cells with poor immunogenicity were used,[24] as ICD process is featured to reverse such poor immunogenicity, making the cancer cells susceptible for immunotherapy.[2] In this experiment, healthy BALB/c mice were randomly divided into 4 groups with each one containing 10 mice, which were named as "Control," "X-ray," "Ce6," and "TPE-DPA-TCyP," respectively. As illustrated in **Figure 4**A, for "TPE-DPA-TCyP" and "Ce6" groups, TPE-DPA-TCyP (0.2×10^{-6} M)-incubated and Ce6 (0.5×10^{-6} M)-incubated 4T1 cancer cells were irradiated by white light (10 mW cm^{-2}, 1 min) to evoke ecto-CRT, respectively, followed by exposure to X-ray (single-fraction irradiation of 60 Gy) to ensure the cancer cells lose their tumorigenicity. For "X-ray" group, 4T1 cancer cells were only attenuated by X-ray (single-fraction irradiation of 60 Gy) without any ICD inducer treatment. Noteworthy, single-fraction irradiation of 60 Gy itself has rather weak ability to induce ICD and nearly no combined ICD effect with PDT by TPE-DPA-TCyP (Figure S37, Supporting Information). This is reasonable because it has been reported that multiple irradiations with low dose (e.g., 8 Gy) is much more effective to induce antitumor immunity of ICD than single irradiation with high dose.[25] Subsequently, the "TPE-DPA-TCyP + X-ray"-treated, "Ce6 + X-ray"-treated, and "X-ray only"-treated 4T1 cancer cells were used as cancer vaccines and we then immunized healthy mice with each vaccine twice on day 0 and day 7 by subcutaneous injection into mouse right axilla. For "Control" group, pure PBS instead of cancer cell vaccine was subcutaneously injected into the healthy mice on day 0 and day 7, respectively. On day 14, each mouse in all 4 groups was challenged with 1×10^6 live 4T1 cancer cells into the left axilla, followed by monitoring the tumor growth for another 32 days.

As shown in Figure 4B, fast 4T1 tumor growth is observed in "Control" cohort because of its high malignance. Encouragingly, excellent inhibition effect in tumor growth can be realized for mice immunized with "TPE-DPA-TCyP + X-ray"-treated cells. Quantitatively, the average tumor volume on day 32 post live cancer cell inoculation in "TPE-DPA-TCyP" group is ≈183 mm^3, 11.5 times smaller than that in "Control" group (≈2105 mm^3). As controls, the vaccines of "Ce6 + X-ray"-treated and "X-ray only"-treated cells fail to suppress the tumor growth as effective as that of "TPE-DPA-TCyP + X-ray"-treated cells, as evidenced by the final average tumor volumes of ≈1870 and ≈1505 mm^3 for "X-ray" and "Ce6" cohorts, respectively. Moreover, 9 of 10 mice in "TPE-DPA-TCyP" group survived 50 days after live cancer cell inoculation, whereas the mice in the other 3 groups all died during this period (Figure 4C). These results verify that TPE-DPA-TCyP-treated cell vaccine is the most efficacious to enhance the capability of mice in resisting challenge with live 4T1 cancer cells. As prophylactic tumor vaccination experiment is a widely accepted method for in vivo ICD evaluation,[1,2] the data reveal that mitochondrial targeting TPE-DPA-TCyP is much superior in ICD induction to Ce6, which has been reported as one of the most effective photosensitizer-based ICD inducers so far.

To essentially understand the underlying mechanism of the aforementioned antitumor immunity, a series of analyses of immune cells were performed. To achieve the final aim to activate the antitumor immunity, the first crucial step is effective

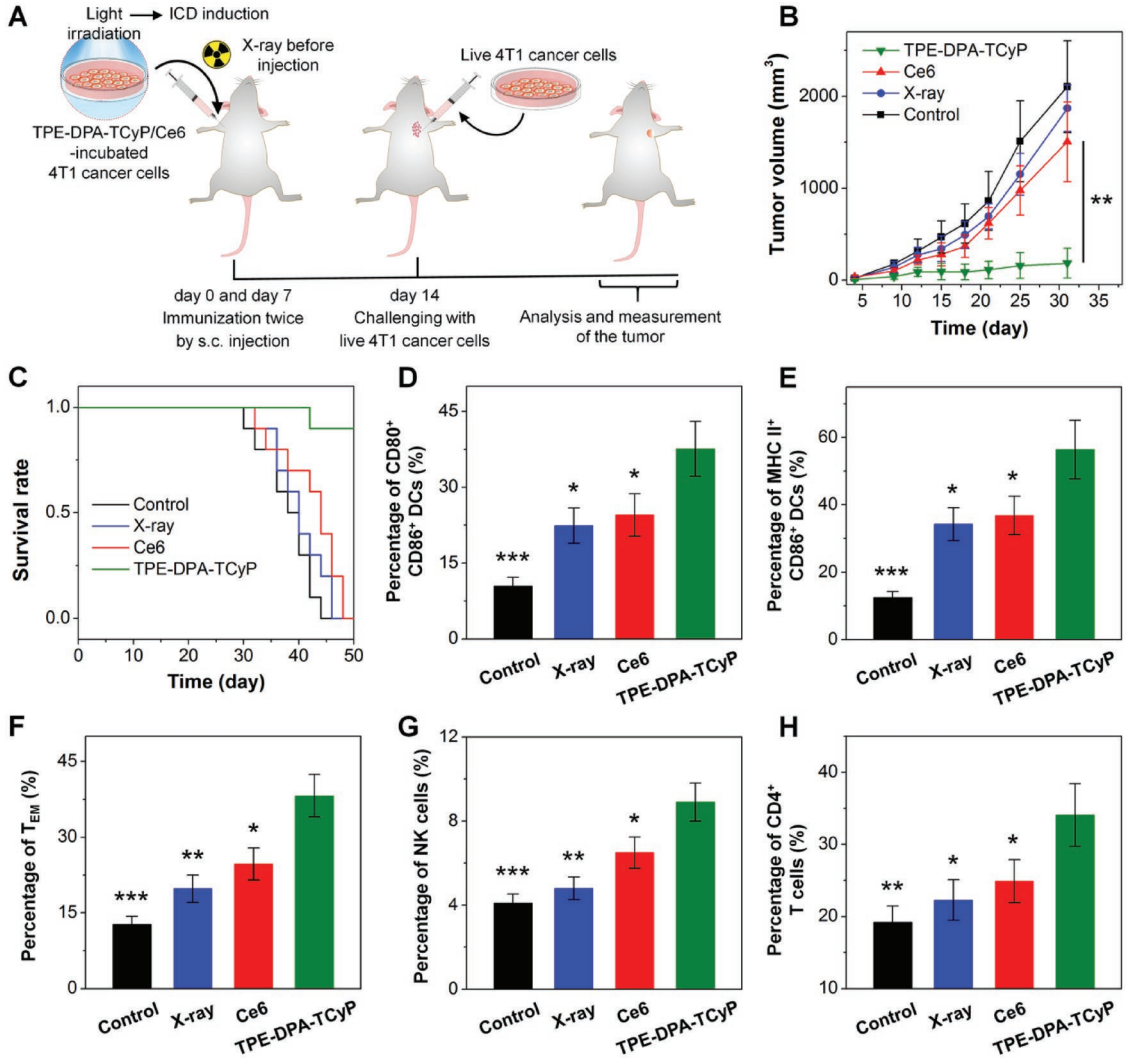

Figure 4. A) Schematic of using a prophylactic tumor vaccination model to evaluate the in vivo ICD immunogenicity of different ICD inducers. The "s.c." represents "subcutaneous." B,C) Plot of tumor volume (B) and survival rate of mice (C) in different groups indicated versus the time post live 4T1 cancer cell inoculation. In (B), Error bars, mean ± SD ($n = 10$). ** $P < 0.01$. D–H) Quantitative analyses of the percentages of $CD80^+CD86^+$ DCs (D), $CD86^+MHC\ II^+$ DCs (E), T_{EM} cells (F), NK cells (G), and $CD4^+$ T cells (H). In (D–H), Error bars, mean ± SD ($n = 4$). *** $P < 0.001$, ** $P < 0.01$, and * $P < 0.05$, in comparison with "TPE-DPA-TCyP" cohort.

initiate adaptive immunity. Therefore, we investigated the significant step of DC maturation and presentation in lymph nodes. On day 14, the mice in each group that were immunized twice on day 0 and day 7 were sacrificed and the axillary lymph nodes were isolated for flow cytometry analysis. The CD80 and CD86 (co-stimulation molecules), as well as major histocompatibility complex class II (MHC II) molecules mark the DC maturation.[26] As displayed in Figure 4D and Figure S38 (Supporting Information), the percentage of $CD80^+$ $CD86^+$ DCs in "TPE-DPA-TCyP" group (≈37%) is significantly higher than those in other 3 groups (≈24%, ≈22%, and ≈11% for "Ce6," "X-ray," and "Control" group, respectively). Meanwhile, as shown in Figure 4E and Figure S39 (Supporting Information), the proportion of $CD86^+$ $MHC\ II^+$ DCs (fully activated DCs)[27] in "TPE-DPA-TCyP" group (≈56%) also has a significant increase when comparing with other 3 groups (≈37%, ≈34%, and ≈13% for "Ce6," "X-ray," and "Control" group, respectively). These results demonstrate that TPE-DPA-TCyP-treated tumor cell vaccine gives the best performance in DC maturation promotion.

The effector memory T cells (T_{EM}) isolated from the spleen were also examined on day 14, which play a pivotal role in elicit immediate protection from inoculated live cancer cells.[28] As shown in Figure 4F and Figure S40 (Supporting Information), the percentage of T_{EM} ($CD3^+$ $CD8^+$ $CD62L^-$ $CD44^+$) in "TPE-DPA-TCyP" group is 1.5-fold and 2.9-fold higher than that in "Ce6" and "Control" groups, respectively, addressing the mechanism of the long-lasting effect of antitumor immunity of TPE-DPA-TCyP-treated cell vaccine. Additionally, $CD8^+$ T cells in spleen were also evaluated, which are tightly closed to the differentiation of T_{EM}.[29] As expected, "TPE-DPA-TCyP" group exhibits the highest percentage of $CD8^+$ T cells (Figures S41 and S42, Supporting Information). Furthermore, the proportions of activated ($CD38^+$) and exhausted ($PD\text{-}1^+$) $CD8^+$ T cells[30] in 4 groups were analyzed. As displayed in Figures S43–S46

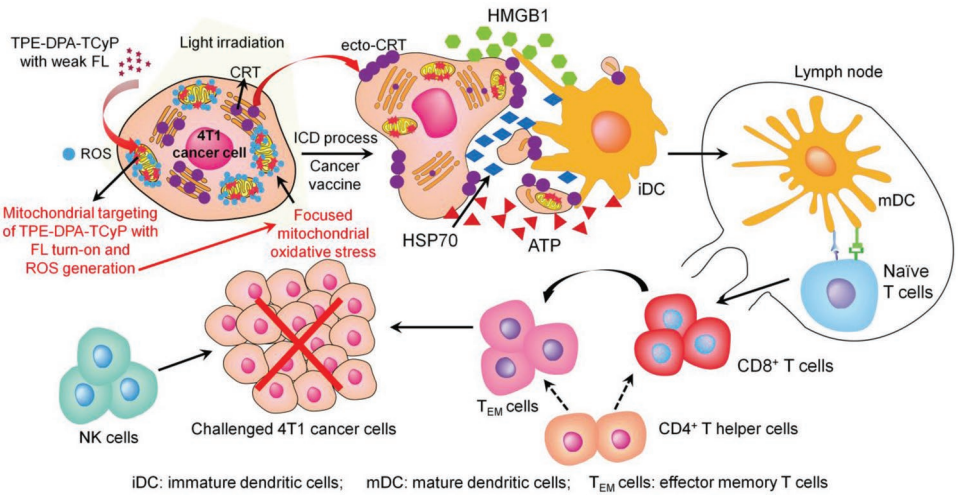

Figure 5. The proposed mechanism of TPE-DPA-TCyP as an effective ICD inducer for antitumor immunity.

(Supporting Information), the percentage of activated $CD8^+$ T cells in "TPE-DPA-TCyP" group is remarkably higher than those in other 3 groups (for example, 1.6-fold higher than that in "Ce6" group), whereas the proportions of exhausted $CD8^+$ T cells in 4 groups show no significant differences.

NK cells ($CD3^-CD49b^+$) are featured with both innate and adaptive immune, which generate cytotoxic molecules and kill tumor cells.[31] The results in Figure 4G and Figure S47 (Supporting Information) indicate that TPE-DPA-TCyP-treated cell vaccine induces much more NK cells (≈8.9%) as compared to "Ce6," "X-ray," and "Control" groups (≈6.5%, ≈4.8%, and ≈4.1%, respectively), which contribute to its strong antitumor immunity. Furthermore, NK cell-derived cytokines are important for the differentiation of $CD4^+$ T cells that can help to maintain the antitumor immunity, which may be the reason why $CD4^+$ T helper cells are also in the highest level for "TPE-DPA-TCyP" group (Figure 4H and Figure S48, Supporting Information). Moreover, regulatory T cells (Tregs; $CD3^+CD4^+CD25^+Foxp3^+$) that hinder the adaptive antitumor immunity[32] were investigated as well, but no significant differences are found among the 4 groups (Figures S49 and S50, Supporting Information).

As a consequence, the mechanism of TPE-DPA-TCyP as an extremely effective ICD inducer for antitumor immunity is proposed in **Figure 5**. Our molecular design endows TPE-DPA-TCyP with specific cancer cell mitochondrial targeting and highly efficient ROS production to induce adequate mitochondrial oxidative stress, which greatly improve ICD induction with massive emission of DAMPs including ecto-CRT, secreted ATP, released HMGB1 and HSP70, thus eliciting the adaptive antitumor immunity through recruitment of DCs as well as promotion of DC maturation, antigen presentation and cytokines secretion.[2] Therefore, both the immunogenicity of 4T1 cancer cells and the efficiency of initiating the adaptive antitumor immunity are highly boosted by our material. Furthermore, after immunization by the TPE-DPA-TCyP-treated tumor cell vaccine, greatly increased T_{EM} cells with the lytic functions including secretion of IFN-γ or perforin inhibit the growth of challenged live 4T1 cancer cells. The elevated T helper cells also accelerate the differentiation into functional memory T cells, maintaining their capabilities of long-term survival and responsiveness to live cancer cells.[33] T helper cells also improve the function of $CD8^+$ T cells, which are closely associated with the differentiation of T_{EM}. Besides, NK cells response is also involved in the antitumor immunity by lytic function and interaction with other immune cells. In a word, thanks to the highly improved ICD induction, TPE-DPA-TCyP-treated tumor cell vaccine provokes a rather strong antitumor immunity in vivo by simultaneously triggering both innate and adaptive immune systems.

In summary, we have introduced an alternative class of photosensitizer-based ICD inducer, which is featured with strong AIE effect and specific ability in inducing focused mitochondrial oxidative stress of cancer cells. It is validated that mitochondrial-anchoring TPE-DPA-TCyP is a superior ICD inducer to the widely reported high-performing ones including Ce6, PPa, and oxaliplatin. The better effectiveness and robustness of TPE-DPA-TCyP in inducing antitumor immunity and immune-memory effect are demonstrated in vivo using the prophylactic tumor vaccination model with immune cell analysis data indicating the underlying mechanism that is, simultaneously triggering both innate and adaptive immune systems. As compared to the currently reported photosensitizer-based ICD inducers, TPE-DPA-TCyP is advantageous due to the distinct molecular design guideline in terms of specific mitochondrial targeting, 3D twisted molecular structure and much separated HOMO–LUMO distribution. For the first time, this study reveals the relationship between mitochondrial oxidative stress and ICD. We thus put forward a new concept that focused mitochondrial oxidative stress can massively evoke ICD. Additionally, this is also the first report that connects two emerging fields AIE and ICD together, and demonstrates AIE to be a desirable platform for developing advanced photosensitizer-based ICD inducers.

Supporting Information

Supporting Information is available from the Wiley Online Library or from the author.

Acknowledgements

C.C. and X.N. contributed equally to this work. This work was supported by the NSFC (51622305 and 51873092), the National Basic Research Program of China (2015CB856503), the Fundamental Research Funds for the Central Universities, Nankai University, the Science and Technology Support Program of Tianjin (16YFZCSY01020) and the Fundamental Research Funds for the Central Universities, Nankai University (63191521, 63171218, and 63191176). All animal experiments were performed according to the guidelines set by Tianjin Committee of Use and Care of Laboratory Animals, and the overall project protocols were approved by the Animal Ethics Committee of Nankai University.

Conflict of Interest

The authors declare no conflict of interest.

Keywords

aggregation-induced emission, cancer immunotherapy, immunogenic cell death inducer, mitochondrial targeting, photosensitizers

Received: July 30, 2019
Revised: October 4, 2019
Published online:

[1] a) D. V. Krysko, A. D. Garg, A. Kaczmarek, O. Krysko, P. Agostinis, P. Vandenabeele, *Nat. Rev. Cancer* **2012**, *12*, 860; b) D. R. Green, T. Ferguson, L. Zitvogel, G. Kroemer, *Nat. Rev. Immunol.* **2009**, *9*, 353; c) Y. Fan, R. Kuai, Y. Xu, L. J. Ochyl, D. J. Irvine, J. J. Moon, *Nano Lett.* **2017**, *17*, 7387; d) C. Wang, Y. Ye, Q. Hu, A. Bellotti, Z. Gu, *Adv. Mater.* **2017**, *29*, 1606036.

[2] a) L. Galluzzi, A. Buqué, O. Kepp, L. Zitvogel, G. Kroemer, *Nat. Rev. Immunol.* **2017**, *17*, 97; b) G. Kroemer, L. Galluzzi, O. Kepp, L. Zitvogel, *Annu. Rev. Immunol.* **2013**, *31*, 51.

[3] a) M. Obeid, A. Tesniere, F. Ghiringhelli, G. M. Fimia, L. Apetoh, J. L. Perfettini, M. Castedo, G. Mignot, T. Panaretakis, N. Casares, D. Métivier, N. Larochette, P. van Endert, F. Ciccosanti, M. Piacentini, L. Zitvogel, G. Kroemer, *Nat. Med.* **2007**, *13*, 54; b) A. Tesniere, L. Apetoh, F. Ghiringhelli, N. Joza, T. Panaretakis, O. Kepp, F. Schlemmer, L. Zitvogel, G. Kroemer, *Curr. Opin. Immunol.* **2008**, *20*, 504; c) Q. Chen, J. Chen, Z. Yang, J. Xu, L. Xu, C. Liang, X. Han, Z. Liu, *Adv. Mater.* **2019**, *31*, 1802228.

[4] a) A. M. Dudek, A. D. Garg, D. V. Krysko, D. D. Ruysscher, P. Agostinis, *Cytokine Growth Factor Rev.* **2013**, *24*, 319; b) S. Musetti, L. Huang, *ACS Nano* **2018**, *12*, 11740; c) A. Serrano-del Valle, A. Anel, J. Naval, I. Marzo, *Front. Cell Dev. Biol.* **2019**, *7*, 50; d) A. Lin, Y. Gorbanev, J. De Backer, J. Van Loenhout, W. Van Boxem, F. Lemière, P. Cos, S. Dewilde, E. Smits, A. Bogaerts, *Adv. Sci.* **2019**, *6*, 1802062.

[5] E. Vacchelli, F. Aranda, A. Eggermont, J. Galon, C. Sautès-Fridman, I. Cremer, L. Zitvogel, G. Kroemer, L. Galluzzi, *OncoImmunology* **2014**, *3*, e27878.

[6] a) C. Pozzi, A. Cuomo, I. Spadoni, E. Magni, A. Silvola, A. Conte, S. Sigismund, P. S. Ravenda, T. Bonaldi, M. G. Zampino, C. Cancelliere, P. P. Di Fiore, A. Bardelli, G. Penna, M. Rescigno, *Nat. Med.* **2016**, *22*, 624; b) K. Kono, K. Mimura, R. Kiessling, *Cell Death Dis.* **2013**, *4*, e688; c) J. Pol, E. Vacchelli, F. Aranda, F. Castoldi, A. Eggermont, I. Cremer, C. Sautès-Fridman, J. Fucikova, J. Galon, R. Spisek, E. Tartour, L. Zitvogel, G. Kroemer, L. Galluzzi, *OncoImmunology* **2015**, *4*, e1008866; d) W. Song, L. Shen, Y. Wang, Q. Liu, T. J. Goodwin, J. Li, O. Dorosheva, T. Liu, R. Liu, L. Huang, *Nat. Commun.* **2018**, *9*, 2237; e) H. Y. Yoon, S. T. Selvan, Y. Yang, M. J. Kim, D. K. Yi, I. C. Kwon, K. Kim, *Biomaterials* **2018**, *178*, 597; f) F. Zhou, B. Feng, H. Yu, D. Wang, T. Wang, Y. Ma, S. Wang, Y. Li, *Adv. Mater.* **2019**, *31*, 1805888.

[7] a) A. Tesniere, F. Schlemmer, V. Boige, O. Kepp, I. Martins, F. Ghiringhelli, L. Aymeric, M. Michaud, L. Apetoh, L. Barault, J. Mendiboure, J. P. Pignon, V. Jooste, P. van Endert, M. Ducreux, L. Zitvogel, F. Piard, G. Kroemer, *Oncogene* **2010**, *29*, 482; b) X. Zhao, K. Yang, R. Zhao, T. Ji, X. Wang, X. Yang, Y. Zhang, K. Cheng, S. Liu, J. Hao, H. Ren, K. W. Leong, G. Nie, *Biomaterials* **2016**, *102*, 187; c) J. Lu, X. Liu, Y. P. Liao, F. Salazar, B. Sun, W. Jiang, C. H. Chang, J. Jiang, X. Wang, A. M. Wu, H. Meng, A. E. Nel, *Nat. Commun.* **2017**, *8*, 1811; d) B. Feng, F. Zhou, B. Hou, D. Wang, T. Wang, Y. Fu, Y. Ma, H. Yu, Y. Li, *Adv. Mater.* **2018**, *30*, 1803001.

[8] a) J. P. van Vloten, S. T. Workenhe, S. K. Wootton, K. L. Mossman, B. W. Bridle, *J. Immunol.* **2018**, *200*, 450; b) E. B. Golden, I. Pellicciotta, S. Demaria, M. H. Barcellos-Hoff, S. C. Formenti, *Front. Oncol.* **2012**, *2*, 88; c) Y. Chao, L. Xu, C. Liang, L. Feng, J. Xu, Z. Dong, L. Tian, X. Yi, K. Yang, Z. Liu, *Nat. Biomed. Eng.* **2018**, *2*, 611; d) A. D. Garg, D. V. Krysko, P. Vandenabeele, P. Agostinis, *Photochem. Photobiol. Sci.* **2011**, *10*, 670; e) C. Wang, L. Xu, C. Liang, J. Xiang, R. Peng, Z. Liu, *Adv. Mater.* **2014**, *26*, 8154; f) Q. Chen, L. Xu, C. Liang, C. Wang, R. Peng, Z. Liu, *Nat. Commun.* **2016**, *7*, 13193; g) Q. Chen, Q. Hu, E. Dukhovlinova, G. Chen, S. Ahn, C. Wang, E. A. Ogunnaike, F. S. Ligler, G. Dotti, Z. Gu, *Adv. Mater.* **2019**, *31*, 1900192.

[9] a) Z. Yang, X. Chen, *Acc. Chem. Res.* **2019**, *52*, 1245; b) A. D. Garg, P. Agostinis, *Photochem. Photobiol. Sci.* **2014**, *13*, 474; c) D. Ni, C. A. Ferreira, T. E. Barnhart, V. Quach, B. Yu, D. Jiang, W. Wei, H. Liu, J. W. Engle, P. Hu, W. Cai, *J. Am. Chem. Soc.* **2018**, *140*, 14971.

[10] a) X. Duan, C. Chan, W. Lin, *Angew. Chem., Int. Ed.* **2019**, *58*, 670; b) Z. Chen, L. Liu, R. Liang, Z. Luo, H. He, Z. Wu, H. Tian, M. Zheng, Y. Ma, L. Cai, *ACS Nano* **2018**, *12*, 8633; c) G. Yang, L. Xu, J. Xu, R. Zhang, G. Song, Y. Chao, L. Feng, F. Han, Z. Dong, B. Li, Z. Liu, *Nano Lett.* **2018**, *18*, 2475.

[11] a) A. D. Garg, L. Vandenberk, C. Koks, T. Verschuere, L. Boon, S. W. Van Gool, P. Agostinis, *Sci. Transl. Med.* **2016**, *8*, 328ra27; b) R. Liang, L. Liu, H. He, Z. Chen, Z. Han, Z. Luo, Z. Wu, M. Zheng, Y. Ma, L. Cai, *Biomaterials* **2018**, *177*, 149; c) C. W. Ng, J. Li, K. Pu, *Adv. Funct. Mater.* **2018**, *28*, 1804688; d) M. Korbelik, *Lasers Surg. Med.* **2018**, *50*, 491; e) L. Lu, C. He, N. Guo, C. Chan, K. Ni, R. R. Weichselbaum, W. Lin, *J. Am. Chem. Soc.* **2016**, *138*, 12502; f) D. Wang, T. Wang, J. Liu, H. Yu, S. Jiao, B. Feng, F. Zhou, Y. Fu, Q. Yin, P. Zhang, Z. Zhang, Z. Zhou, Y. Li, *Nano Lett.* **2016**, *16*, 5503.

[12] M. Korbelik, J. Banáth, K. M. Saw, W. Zhang, E. Čiplys, *Front. Oncol.* **2015**, *5*, 15.

[13] a) C. He, X. Duan, N. Guo, C. Chan, C. Poon, R. R. Weichselbaum, W. Lin, *Nat. Commun.* **2016**, *7*, 12499; b) G. Lan, K. Ni, Z. Xu, S. S. Veroneau, Y. Song, W. Lin, *J. Am. Chem. Soc.* **2018**, *140*, 5670; c) Q. Chen, C. Wang, G. Chen, Q. Hu, Z. Gu, *Adv. Healthcare Mater.* **2018**, *7*, 1800424; d) G. Yang, L. Xu, Y. Chao, J. Xu, X. Sun, Y. Wu, R. Peng, Z. Liu, *Nat. Commun.* **2017**, *8*, 902; e) J. Xu, L. Xu, C. Wang, R. Yang, Q. Zhuang, X. Han, Z. Dong, W. Zhu, R. Peng, Z. Liu, *ACS Nano* **2017**, *11*, 4463.

[14] a) H. Gao, X. Zhang, C. Chen, K. Li, D. Ding, *Adv. Biosyst.* **2018**, *2*, 1800074; b) J. F. Lovell, T. W. B. Liu, J. Chen, G. Zheng, *Chem. Rev.* **2010**, *110*, 2839; c) W. Fan, P. Huang, X. Chen, *Chem. Soc. Rev.* **2016**, *45*, 6488.

[15] a) X. Ni, X. Zhang, X. Duan, H. L. Zheng, X. S. Xue, D. Ding, *Nano Lett.* **2019**, *19*, 318; b) G. Feng, B. Liu, *Acc. Chem. Res.* **2018**,

51, 1404; c) K. Gu, W. H. Zhu, X. Peng, *Sci. China: Chem.* **2019**, *62*, 189.

[16] a) C. Chen, H. Ou, R. Liu, D. Ding, *Adv. Mater.* **2019**, *31*, 1806331; b) K. Han, S. B. Wang, Q. Lei, J. Y. Zhu, X. Z. Zhang, *ACS Nano* **2015**, *9*, 10268; c) J. Qi, C. Chen, D. Ding, B. Z. Tang, *Adv. Healthcare Mater.* **2018**, *7*, 1800477.

[17] L. Galluzzi, T. Yamazaki, G. Kroemer, *Nat. Rev. Mol. Cell Biol.* **2018**, *19*, 731.

[18] a) R. B. Hamanaka, N. S. Chandel, *Trends Biochem. Sci.* **2010**, *35*, 505; b) A. R. van Vliet, T. Verfaillie, P. Agostinis, *Biochim. Biophys. Acta – Mol. Cell Res.* **2014**, *1843*, 2253; c) L. A. Sena, N. S. Chandel, *Mol. Cell* **2012**, *48*, 158.

[19] C. Y. Y. Yu, H. Xu, S. Ji, R. T. K. Kwok, J. W. Y. Lam, X. Li, S. Krishnan, D. Ding, B. Z. Tang, *Adv. Mater.* **2017**, *29*, 1606167.

[20] S. Xu, Y. Yuan, X. Cai, C. J. Zhang, F. Hu, J. Liang, G. Zhang, D. Zhang, B. Liu, *Chem. Sci.* **2015**, *6*, 5824.

[21] a) J. Qi, C. Chen, X. Zhang, X. Hu, S. Ji, R. T. K. Kwok, J. W. Y. Lam, D. Ding, B. Z. Tang, *Nat. Commun.* **2018**, *9*, 1848; b) K. Pu, J. Mei, J. V. Jokerst, G. Hong, A. L. Antaris, N. Chattopadhyay, A. J. Shuhendler, T. Kurosawa, Y. Zhou, S. S. Gambhir, Z. Bao, J. Rao, *Adv. Mater.* **2015**, *27*, 5184; c) J. E. Lemaster, Z. Wang, A. Hariri, F. Chen, Z. Hu, Y. Huang, C. V. Barback, R. Cochran, N. C. Gianneschi, J. V. Jokerst, *Chem. Mater.* **2019**, *31*, 251; d) C. Moore, J. V. Jokerst, *Theranostics* **2019**, *9*, 1550.

[22] Q. Miao, C. Xie, X. Zhen, Y. Lyu, H. Duan, X. Liu, J. V. Jokerst, K. Pu, *Nat. Biotechnol.* **2017**, *35*, 1102.

[23] a) L. Bezu, A. Sauvat, J. Humeau, L. C. Gomes-da-Silva, K. Iribarren, S. Forveille, P. Garcia, L. Zhao, P. Liu, L. Zitvogel, L. Senovilla, O. Kepp, G. Kroemer, *Cell Death Differ.* **2018**, *25*, 1375; b) O. Kepp, L. Menger, E. Vacchelli, C. Locher, S. Adjemian, T. Yamazaki, I. Martins, A. Q. Sukkurwala, M. Michaud, L. Senovilla, L. Galluzzi, G. Kroemer, L. Zitvogel, *Cytokine Growth Factor Rev.* **2013**, *24*, 311.

[24] C. Wang, J. Wang, X. Zhang, S. Yu, D. Wen, Q. Hu, Y. Ye, H. Bomba, X. Hu, Z. Liu, G. Dotti, Z. Gu, *Sci. Transl. Med.* **2018**, *10*, eaan3682.

[25] M. Z. Dewan, A. Galloway, N. Kawashima, J. K. Dewyngaert, J. Babb, S. Formenti, S. Demaria, *Clin. Cancer Res.* **2009**, *15*, 5379.

[26] Q. Chen, C. Wang, X. Zhang, G. Chen, Q. Hu, H. Li, J. Wang, D. Wen, Y. Zhang, Y. Lu, G. Yang, C. Jiang, J. Wang, G. Dotti, Z. Gu, *Nat. Nanotechnol.* **2019**, *14*, 89.

[27] C. Egelston, J. Kurkó, T. Besenyei, B. Tryniszewska, T. A. Rauch, T. T. Glant, K. Mikecz, *Arthritis Rheum.* **2012**, *64*, 3179.

[28] Q. Hu, W. Sun, J. Wang, H. Ruan, X. Zhang, Y. Ye, S. Shen, C. Wang, W. Lu, K. Cheng, G. Dotti, J. F. Zeidner, J. Wang, Z. Gu, *Nat. Biomed. Eng.* **2018**, *2*, 831.

[29] S. M. Kaech, E. J. Wherry, R. Ahmed, *Nat. Rev. Immunol.* **2002**, *2*, 251.

[30] C. Haymaker, R. C. Wu, C. Bernatchez, L. G. Radvanyi, *OncoImmunology* **2012**, *1*, 735.

[31] A. Moretta, E. Marcenaro, S. Parolini, G. Ferlazzo, L. Moretta, *Cell Death Differ.* **2008**, *15*, 226.

[32] H. Nishikawa, S. Sakaguchi, *Int. J. Cancer* **2010**, *127*, 759.

[33] J. C. Sun, M. A. Williams, M. J. Bevan, *Nat. Immunol.* **2004**, *5*, 927.